

Contract No.:

This manuscript has been authored by Savannah River Nuclear Solutions (SRNS), LLC under Contract No. DE-AC09-08SR22470 with the U.S. Department of Energy (DOE) Office of Environmental Management (EM).

Disclaimer:

The United States Government retains and the publisher, by accepting this article for publication, acknowledges that the United States Government retains a non-exclusive, paid-up, irrevocable, worldwide license to publish or reproduce the published form of this work, or allow others to do so, for United States Government purposes.

Bronze Alloy Development for Zinc Vapor Capture

Abstract

After gamma emitting ^{65}Zn was detected in a vacuum pumping system contained in a tritium glovebox, a series of experiments were undertaken to develop a method and material to trap zinc vapors in an area that is more suitable for preventing dose to workers. In this study, bronze alloys with 0 to 30 % tin were prepared using a powder metallurgical process and exposed to three levels of zinc vapors. All of the alloys demonstrated acceptable zinc gettering capacity, however, low tin content bronzes are considered for further testing.

Background

Gamma emitting contamination of ^{65}Zn (Zn) deposits were detected in a vacuum pumping system after a thermal treatment of irradiated components that are used for tritium production (1). Select deposits were analyzed and it was determined that the source of the contamination was vapor deposition of small amounts of activated zinc from residual elements in the irradiated objects. The deposits were characterized for shape, formation, and adhesion as described in Ref. (1). The results indicate that the ^{65}Zn is derived from activated natural zinc and migrates as a metallic vapor. (1).

As a result of conducting a number of experiments, a method to trap zinc vapors using filters that were heated to a specific temperature and placed strategically in the process piping was developed (2). This solution, although effective for low tritium production rates creates challenges at increased production rates since the gamma emitting zinc is captured in a glovebox that is designed to contain gaseous radioactive materials. Consequently, the facility operators desired a solution for this problem that is more compatible in an area of the facility designed for harder radioisotopes. This area has limited ability to change pressure and temperature profiles. To ensure the quality of the product, any material selected for evaluation could not absorb hydrogen and had to be otherwise compatible with the process. A comprehensive review of materials was conducted and essentially two alloy systems – copper and cobalt based – were compatible with the criteria (3).

Subsequently, a series of experiments was conducted to validate the usefulness of copper and commercial off-the-shelf bronze materials (4). While these materials were successful at capturing zinc vapor, they contain higher than acceptable levels of phosphorus, lead or other species that are incompatible with the process and process gas (5). Consequently, an alloy development program was undertaken to develop a binary alloy from pure powders. Powders were blended, compressed into pellets, sintered, and then tested for zinc capture in the apparatus described in Ref. (4). The alloys ranged in composition from pure copper to 30 weight percent tin (Sn). The pellets with higher weight percent tin resulted in lower melting point alloys, and the hypothesis was that the gettering capability for zinc would scale with melting temperature; i.e., more

effective gettering would occur at lower melting temperatures.

Experimental Approach

Copper powder in the form of flakes was obtained from Fischer Scientific. The powder had a size of $< 10 \mu\text{m}$ and a purity of 99.9%. The common contaminants were not listed. The powder morphology shown in Fig. 1 has a flake shape with unfavorable compaction characteristics.

Tin powder in the form of small diameter spherical powder was obtained from Fischer Scientific. The powder has a diameter of $5 \mu\text{m}$ in order to enhance the opportunity for chemical uniformity after diffusion.

The powders were blended in a high speed ball mixer (Fig. 2) with three to six steel balls with diameters between six to 12 mm present to improve the homogeneity. A few experiments were conducted to determine an effective mixing protocol, but the process was not optimized. The composition of the powder blends ranged from 0 to 30% Sn.

Test articles were prepared by pressing 13 mm pellets in a carbon steel die (Fig. 3) and a simple hydraulic bearing press, shown in Fig. 4. The pellets ranged in thickness from 0.4 to 6 mm. The compaction stress ranged from 3 to $6 \text{ kN} / \text{mm}^2$ (5). Zinc stearate was used as a die lubricant. The first group of samples showed greater thicknesses. With project evolution, the thicknesses were reduced to help improve the surface area to volume ratio.

Pressed samples were sintered in an argon atmosphere in a quartz tube furnace. The samples were placed in the furnace and after sufficient purge time, the furnace was heated using the following procedure: RT to 120°C at $5^\circ\text{C}/\text{min}$; hold for 1 hour; 120 to 220°C at $5^\circ\text{C}/\text{min}$; hold for 2 hours; 220°C to diffusion temp at $5^\circ\text{C}/\text{min}$; hold for 2 hours; and furnace cool. The first step is intended to remove any adsorbed moisture from the powder compact, the second to allow for some solid state tin diffusion and the third to encourage chemical homogenization. The diffusion temperature was based on the equilibrium melting temperature of the alloy blend based on the copper - tin phase diagram (6), shown in Fig. 5. The diffusion temperatures for these experiments were also determined from the phase diagram and were intended to produce 25% liquid. Table 1 contains the typical and actual compositions, liquidus temperature and nominal sintering temperatures between 80 and 90% of the melting point.

Zinc exposure was accomplished by placing the sintered pellets in the high vacuum zinc thermal vaporization and exposure apparatus, and exposing samples heated to 350°C to zinc vapors which were generated by heating the zinc source to 350°C for four hours (4).

The samples were characterized by determining the specific mass gain, color change, brass alloying layer, scanning electron microscopy (SEM) and X-ray energy dispersion spectroscopy (XEDS).

Results and Discussion

The powder blending protocol resulted in a well-blended powder with no appearance of agglomeration of the tin in the copper. An SEM image of a 5% Sn blended powder is shown in Fig. 6, where the bright powder is the tin.

The as-pressed (green) pellets are shown in Fig. 7. These 13 mm pellets were compacted to a force of nominally 44 kN. The copper powder with the flake morphology presented challenges to pressing. The force required to compact the powders was significantly higher forces than had they been spherical (8). The green density for the compacts are listed in Table 2. The appearance after sintering reveals that the amount of tin affects the color of the pellet with more tin causing the orange of the copper to be “washed” out with a metallic gray color. The 30% bronze samples are gray. The sintered density is also listed for the average of the last samples pressed and sintered in the conditions listed. Note that the actual sintering temperature depends on the alloy composition with the goal that the sintering temperature ranges between 85 and 95% of the liquidus temperature as indicated in Fig. 5.

The sintering cycle for several Cu-10wt % Sn pellets is shown in Fig. 8, and the various sintering temperatures are clearly indicated. The other pellets were sintered using the same initial temperatures with only the final temperature varying. Typical sintered samples for each composition from 0 to 30% Sn are shown in Fig. 9. These pellets show colorations that range from the reddish copper color to a yellow bronze color to a gray color at 30% Sn.

Copper and bronze samples from 0 to 30% Sn were exposed to low (TC10), medium (TC8), and high (TC1) zinc fluxes, where TC indicates the location of thermocouples in the reaction chamber with TC1 being near the zinc source and each increasing value being 31.75 mm above the zinc source. While, these terms are somewhat nebulous, they reflect the relative amount of zinc that was deposited on the samples. The surface condition of all the samples is shown in Fig. 10. The low flux and medium flux samples changed color from the orange tint of bronze to a yellow/gold brass coloration for the samples that contained 20% Sn or less and the higher alloyed samples remained gray. The samples exposed to the high flux of zinc all turned gray. The cross sections of selected samples were examined using optical and scanning electron microscopy. The specific mass gain (mg/cm^2) for these samples was determined. The various flux amounts are correlated with the filter temperatures as shown in Fig. 11. These data show fairly consistent zinc capture as a function of tin content across the range tested. The cross sections shown in Fig. 12 indicate that these samples exhibit a dense surface for the low flux (TC8) condition and a composition of nominally 40% Zn for the 5, 10, and 20% Sn samples. There was very little difference between the samples with varying Sn composition. The high flux samples (TC1) contain approximately 50% Zn for the 10 and 20% Sn samples. For both the low and high flux samples, there was very little Zn below the reaction layer.

Conclusions

Based on the results of this study, there is not a measureable effect of Sn content on the zinc gettering capability of powder metallurgically processed bronze. The zinc capture capability depends on the zinc flux and the substrate temperature; these effects are not readily separated based on the zinc deposition apparatus. Further development and testing of low tin content bronzes is warranted to allow for cold working to maximize the surface area of the getters.

Acknowledgements

Many people supported this work including Melissa Golyski and Adrian Mendez-Torres who provided SEM data and services, Craig Stripling who provided general laboratory support,

References

1. P. S. Korinko and M.H. Tosten, “Analysis of Zinc 65 Contamination after Vacuum thermal Process”, Journal of Failure Analysis and Prevention, Vol. 13, No. 4, 389-395., Aug. 2013.
2. Paul S. Korinko, Andrew J. Duncan, Kevin J. Stoner, Methods of Preventing the Spread of Zinc Contamination During Vacuum Processing, Journal of Failure Analysis and Prev, Dec. 2013.
3. P.S. Korinko, Zinc Mitigation Interim Report – Thermodynamic Study, Report SRNL-STI-2010-00473, Dec 17, 2010 (available from Department of Energy – Office of Science and Technology Information, <http://www.osti.gov/scitech/>).
4. P.S. Korinko, Zinc vapor trapping using copper based materials, Journal of Failure Analysis and Prevention, Vol 16, #3, 2016.
5. Preparation of Bronze by Powder Metallurgy
6. Copper Tin Phase Diagram, ASM International
7. P.S. Korinko, S. M. Hunyadi Murph, G. Larsen, Tritium Contamination Prevention Using Sacrificial Materials, Fusion Science and Technology, accepted for publication
8. R.M. German, Powder Metallurgy, Metal Powder Industry, 1984, Princeton, NJ



Figure 1. Photo of the plenary powder mixer used to blend the elemental powders.



Figure 2. 13 mm pellet die used to compact the green powders.



Figure 3. Hydraulic Press used to compact the powders to a force of ? N

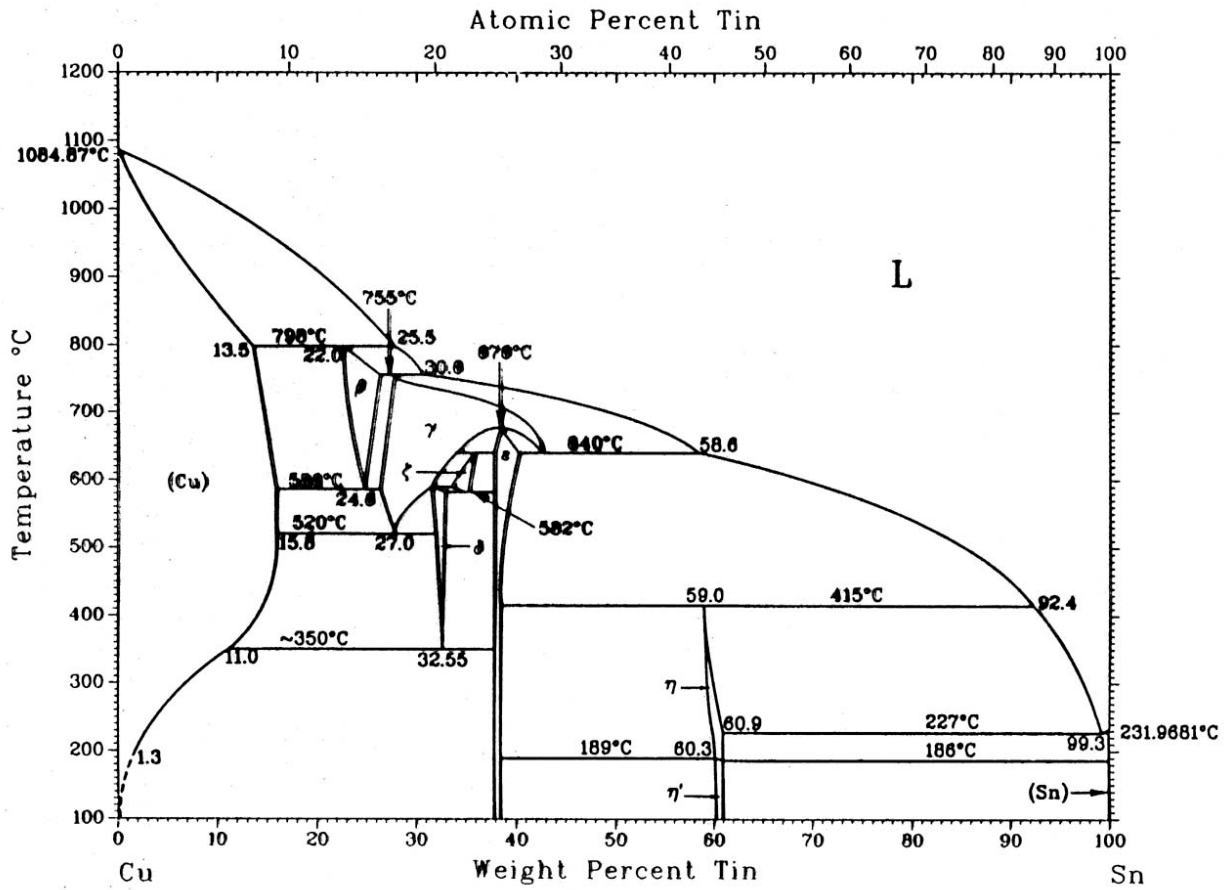


Figure 4. Cu – Sn phase diagram from ASM Handbook

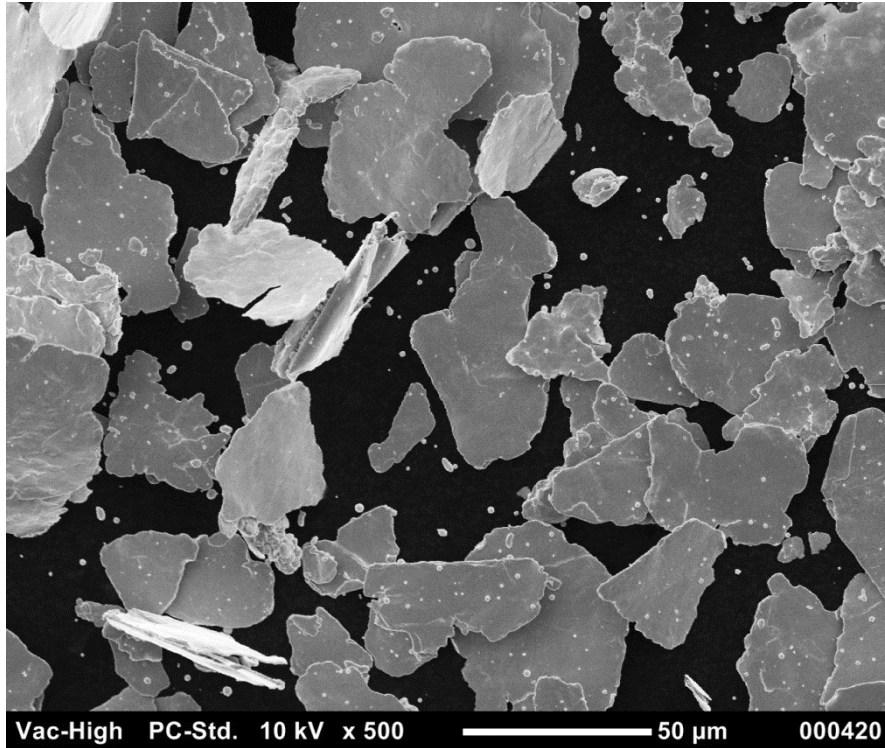


Figure 5. SEM image of Cu + 5 Sn powder blend, note the flake appearance of the Cu powder and fine bright particles of Sn.

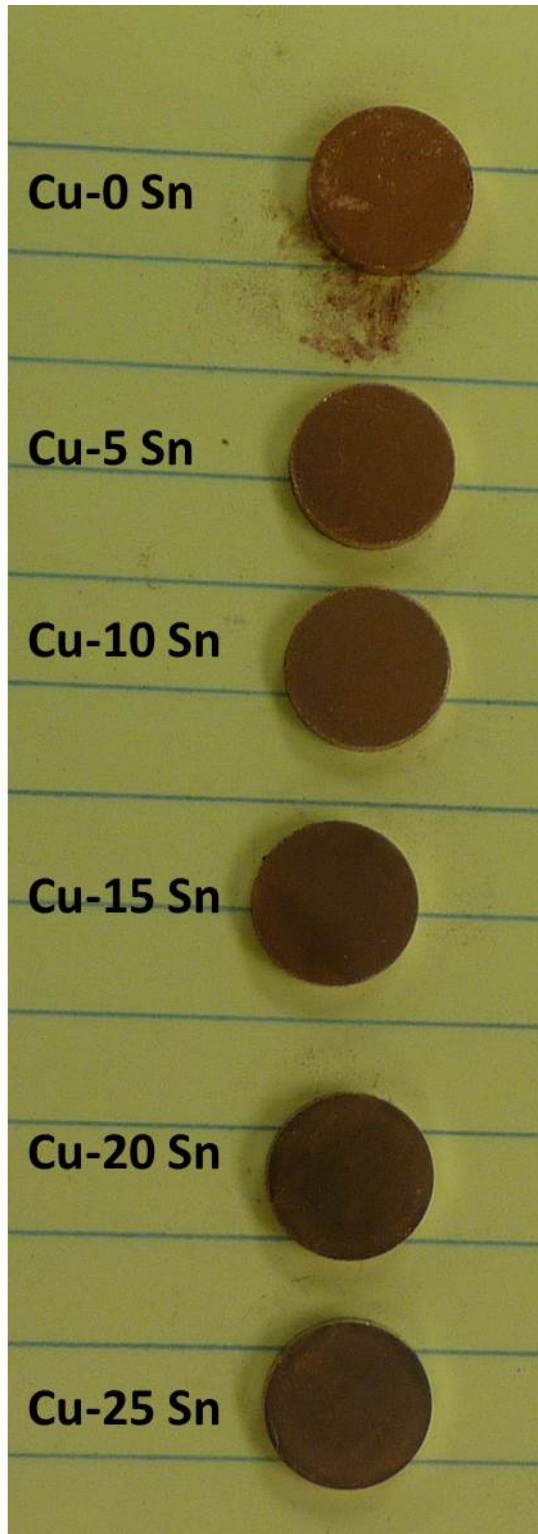


Figure 6. Green pressed pellets of Cu with 0 to 25 Sn.

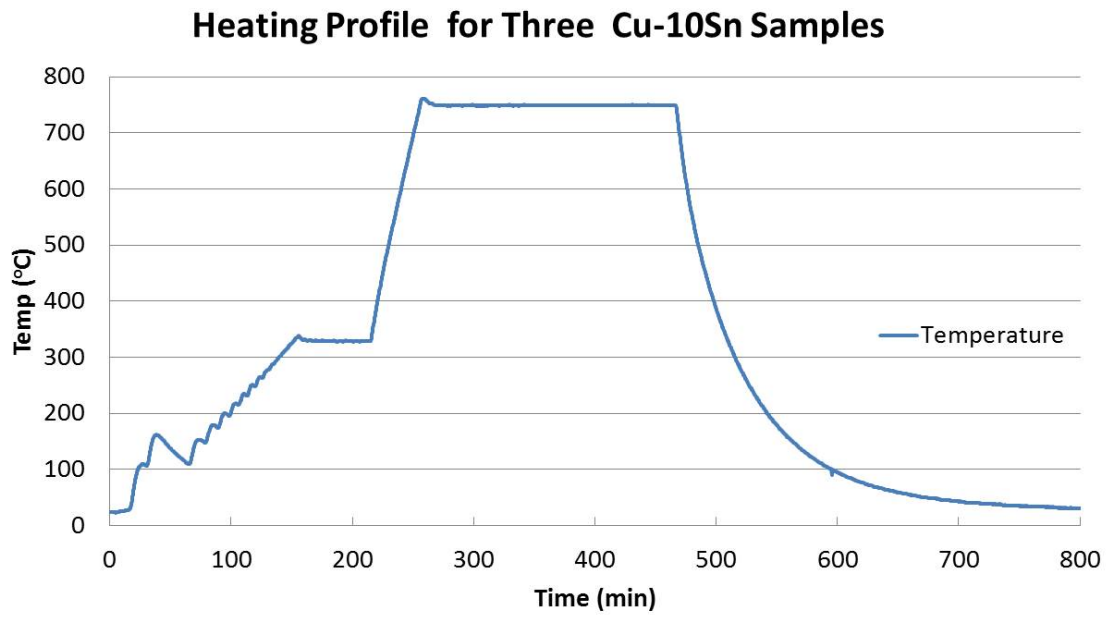


Figure 7. Typical sintering cycle for Cu-10 Sn samples.



Figure 8. Typical appearance of Cu – Sn pellets from 0 to 30%.

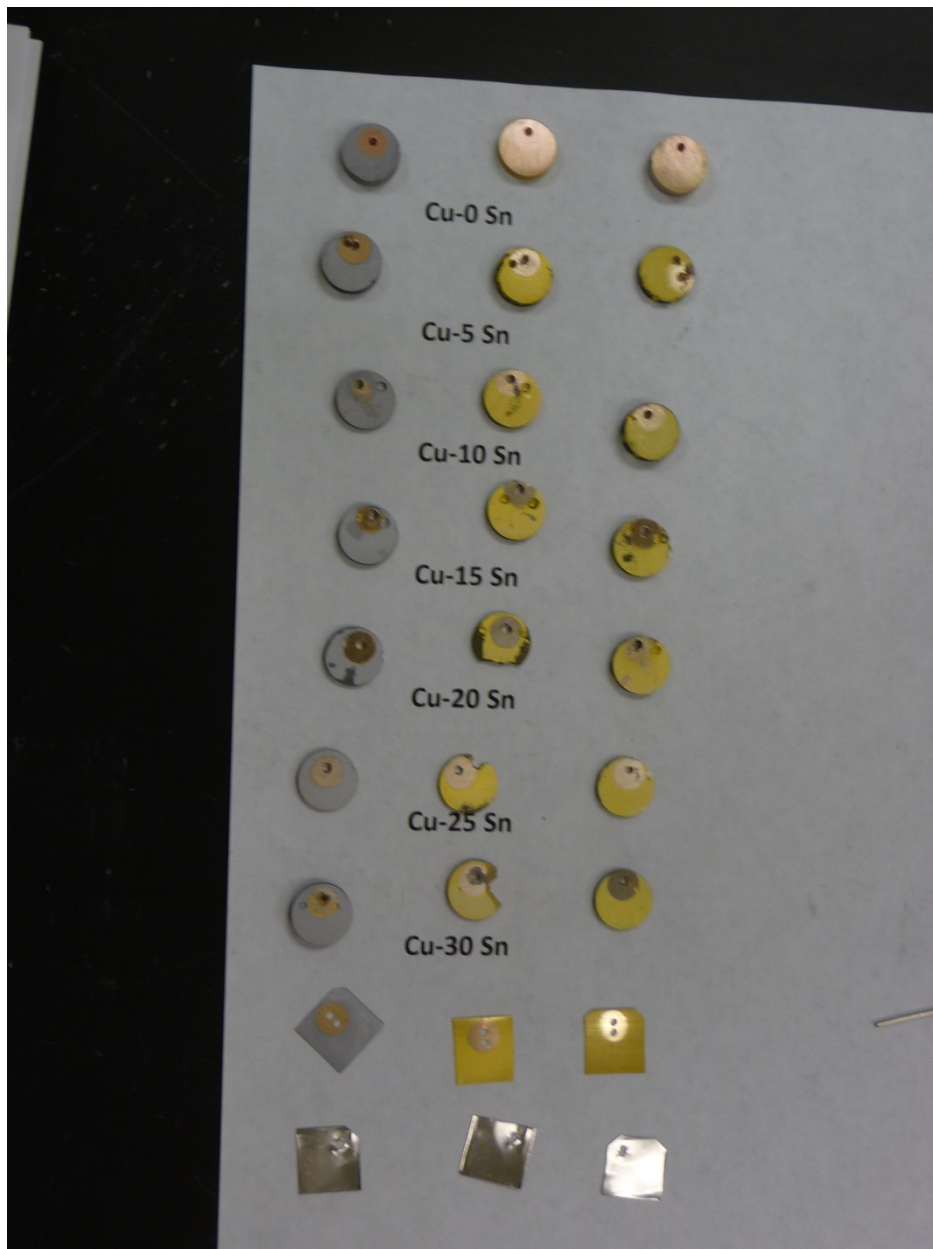


Figure 9. 0- 30% Sn pellet samples and bronze and stainless steel sheets exposed at low, medium and high zinc vapor flux, the circular areas indicate masked areas due to support material.

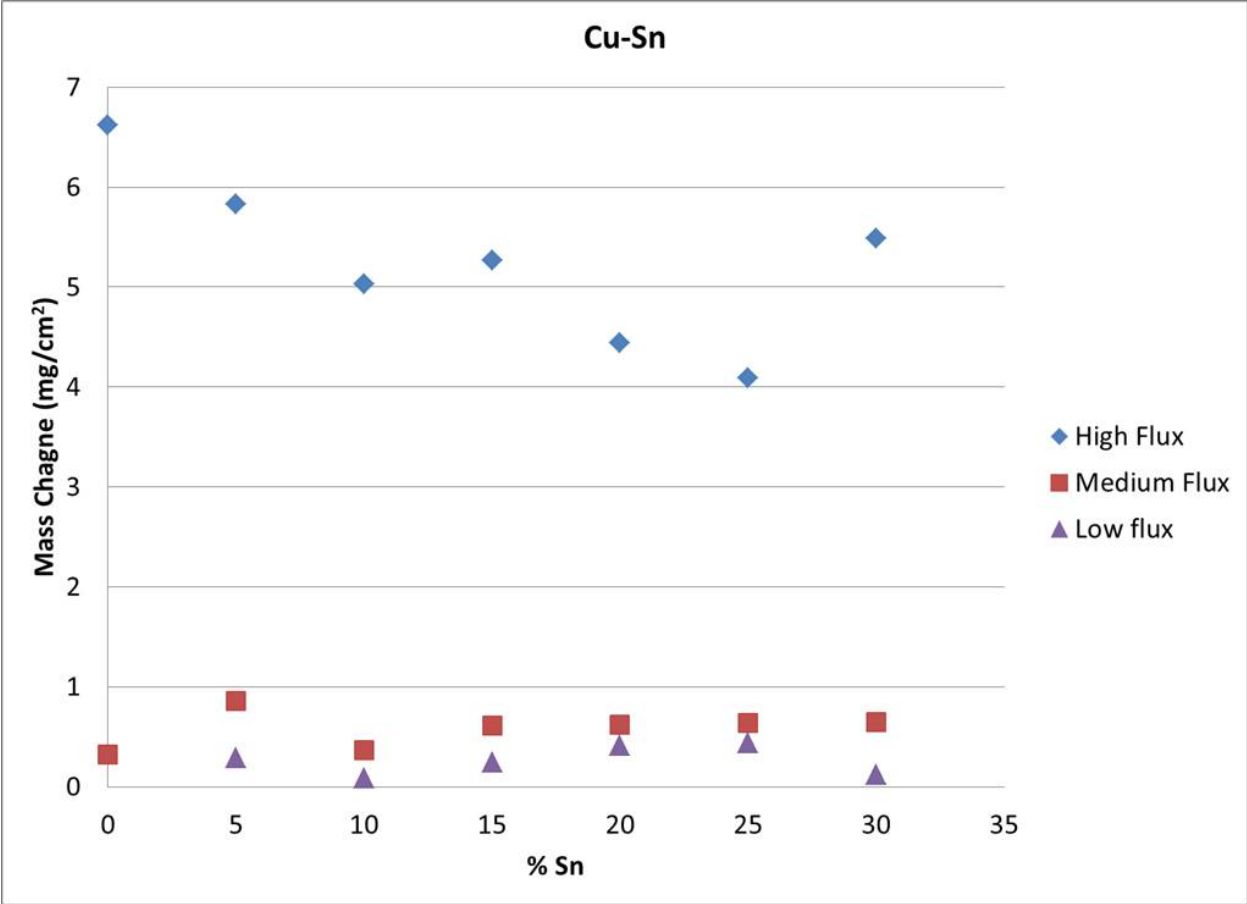


Figure 10. Specific mass change for the three flux levels and across the bronze alloy ranges.

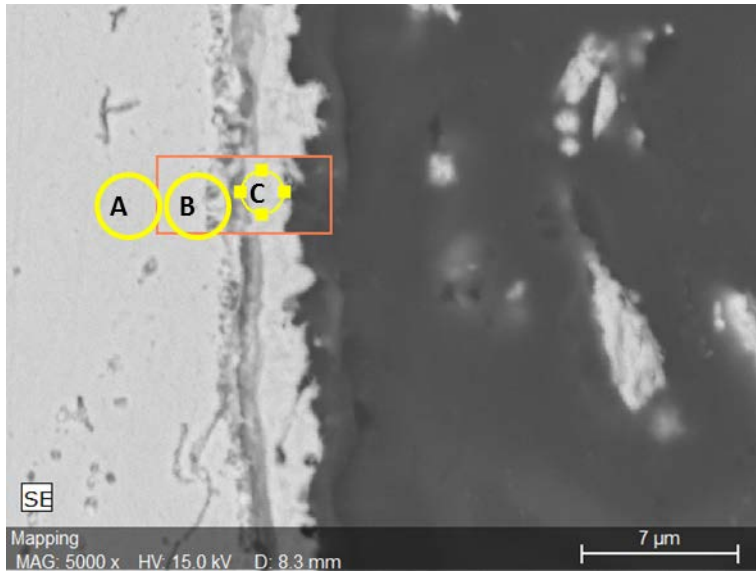


Fig. 11 a

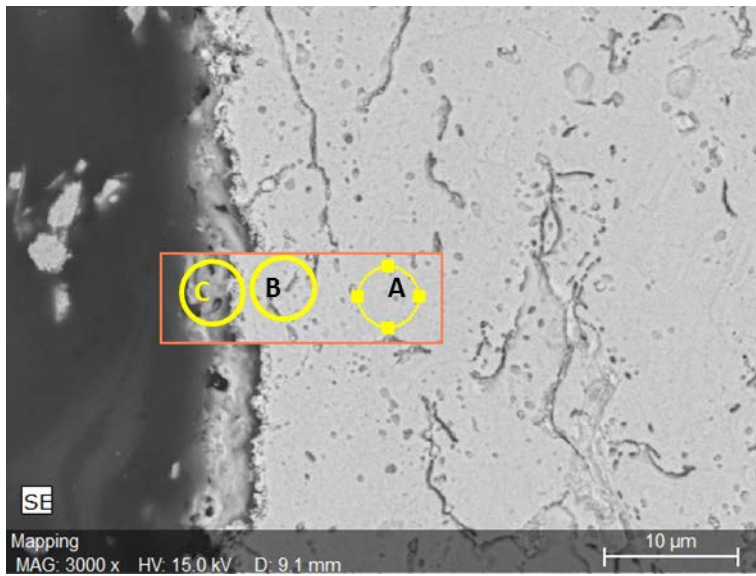


Fig 11b

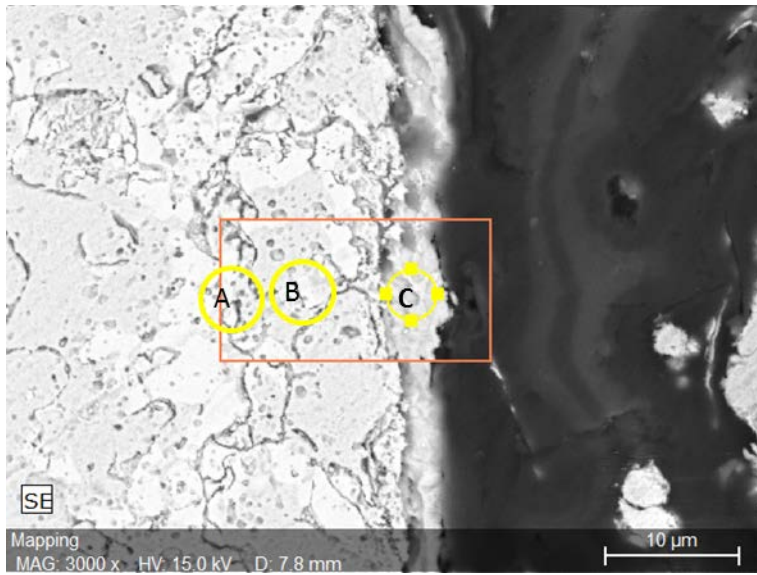


Fig 11c

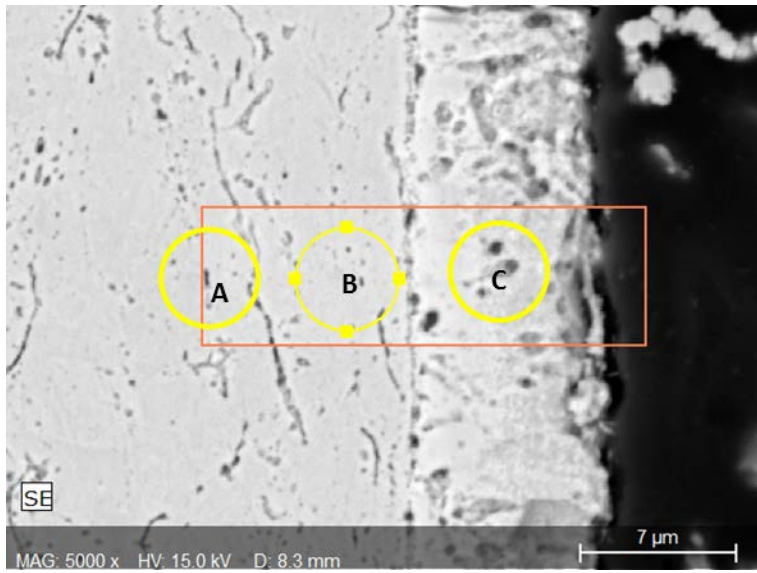


Fig. 11d

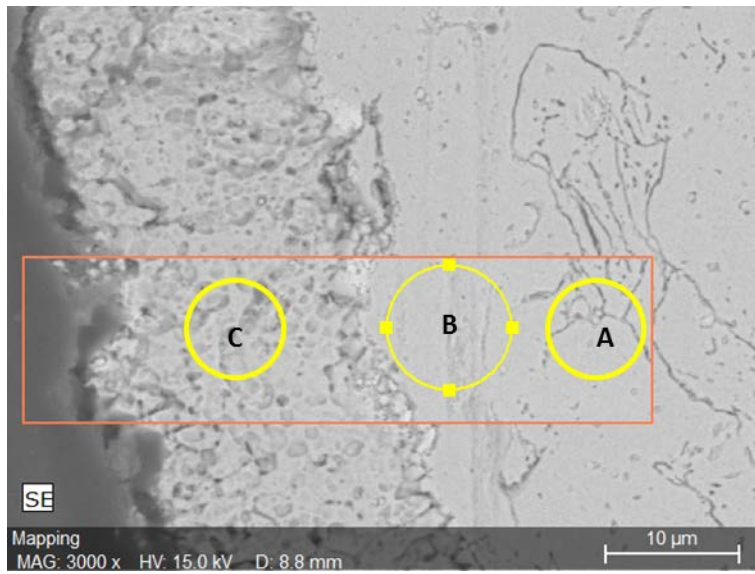


Fig 11e

Figure 11. SEM images of samples that were exposed to medium and high zinc fluxes, a) Cu-5 Sn medium, b) Cu-10 Sn medium, c) Cu-20 Sn medium, d) Cu-5Sn high e) Cu-10 Sn high. The locations indicated on each image shows the composition listed in Table 3.

Table 1. Target and actual compositions for the zinc getter materials

	Target Sn	Target Cu	Density (g/cc)	Actual Sn	Actual Cu	Alloy % Sn
Cu-0Sn	0.000	10.000	8.940	0.000	10.000	0.000
Cu-5 Sn	0.900	17.100	8.841	0.902	17.081	5.017
Cu-10 Sn	1.800	16.200	8.745	2.489	22.446	9.982
Cu-15 Sn	1.500	8.500	8.651	2.703	15.310	15.003
Cu-20 Sn	2.000	8.000	8.558	4.993	19.976	19.997
Cu-25 Sn	2.900	7.100	8.397	4.491	13.488	24.979
Cu-30 Sn	3.000	7.000	8.379	2.977	6.962	29.951

Table 2. Green and sintered density and sintering conditions for the zinc getters

ID	Green Density (%)	Liquidus (°C)	Sintering Temp (°C)	Ts/Tm	Sintered Density (%)	Compaction Stress (MPa)
Cu-0 Sn	82.04	1084	850	0.83	74.27	343.59
Cu-5 Sn	81.99	1060	900	0.88	60.51	341.23
Cu-10 Sn	86.45	1012	830	0.86	53.21	356.36
Cu-15 Sn	87.73	960	770	0.85	53.08	359.72
Cu-20 Sn	91.53	910	770	0.88	46.33	349.64
Cu-25 Sn	92.51	853	740	0.90	65.98	369.81
Cu-30 Sn	88.72	710	700	0.99	86.03	357.48

Table 3. Composition of the deposits formed at two locations in the zinc deposition chamber. Locations are shown in Figure 11, where A is in the substrate, B slightly below the zinc deposit, C in the zinc rich deposit.

Sample ID / Location	Cu	Sn	Zn
Cu-5Sn A Med. Flux	95.61	3.24	1.16
Cu-5Sn B Med. Flux	72.76	5.81	21.43
Cu-5Sn C Med. Flux	56.10	0	43.90
Cu-10Sn A Med. Flux	90.91	8.49	0.60
Cu-10Sn B Med. Flux	85.87	10.17	4.05
Cu-10Sn C Med. Flux	55.64	7.28	37.08
Cu-20Sn A Med. Flux	79.95	19.45	0.60
Cu-20Sn B Med. Flux	78.18	19.29	2.53
Cu-20Sn C Med. Flux	53.58	0.89	45.53
Cu-5Sn A High Flux	94.26	4.82	0.92
Cu-5Sn B High Flux	94.25	3.96	1.79
Cu-5Sn C High Flux	47.30	1.21	51.48
Cu-10Sn A High Flux	86.87	9.57	3.56
Cu-10Sn B High Flux	86.79	10.54	2.66
Cu-10Sn C High Flux	42.26	3.80	53.95